Climate driven trends in London's urban heat island intensity reconstructed over 70 years using a generalized additive model

R. Bassett [a,b,c,*], V. Janes-Bassett [a,b,c], J. Phillipson [b,c], P.J. Young [a,c], G.S. Blair [b,c]

[a] Lancaster Environment Centre, Lancaster University, UK
[b] School of Computing and Communications, Lancaster University, UK
[c] Centre of Excellence in Environmental Data Science, A Joint Centre With the UK Centre for Ecology & Hydrology (UKCEH), Lancaster University, UK

ARTICLE INFO

ABSTRACT

Long-term urban heat island (UHI) observations are uncommon and where available, are generally unable to distinguish changing climate drivers from urban expansion; neither driver is treated independently. We overcome this limitation using a generalized additive model to learn the variability in UHI intensity (UHII) at a central London weather station (St James's Park) over a 10-year observation period (2010–2019). We then use the model to reconstruct 70 years (1950–2019) of monthly night-time UHII variability using ERA5 reanalysis data both as a reference in UHII calculation and for the predictors. We find considerable variability both seasonally and annually within the UHII time series (monthly mean maximum UHIIs are 1.4–2.9 °C). Applying extreme value analysis to the time series we show that monthly mean maximum UHIIs are likely to exceed 2.75 °C once every 11 years. Considering that most studies observe or model UHIIs for less than a year, they will likely misrepresent this UHII variability. Nevertheless, despite moving to a warmer background climate, London's UHII has not significantly changed across the period of analysis (1950–2019). The data-driven methods we create in this study are easily transferable to other cities.

1. Introduction

The local warming from urban modifications to the Earth's surface, known as the urban heat island (UHI) effect, can adversely impact our health and infrastructure (e.g. Santamouris, 2020). While there has been substantial research into UHIs (Masson et al., 2020), in concert with unrelenting global urbanisation, many knowledge gaps remain. Key among these is the inability to define adequate UHI climatologies. Most UHI studies are too short in length to define climatologies, lasting only days, with long-term studies being rare, stemming from difficulties taking representative urban observations. Where long-term studies exist, they are unable to distinguish between the key drivers of UHI change over time: (i) urban morphology and/or (ii) climate. Notwithstanding, state-of-the-art data science methods exist and these can be applied to the urban climate field to address these limitations. Here, we create a methodology using a Generalized Additive Model (GAM) to separate the impacts of these two drivers, and use it to reconstruct a 70-year monthly UHI intensity (UHII; urban minus non-urban temperature difference) time-series in London, UK, that is driven solely by changes in climate. GAMs are an emerging data-science method that can learn complex, non-parametric relationships in data and deal

---

with many predictors, while retaining a strong interpretability of results. GAMs are an extension of generalized linear models that apply non-linear (if present) smoothing functions to the predictors before combining them. They have a diverse range of applications within the environmental sciences, such as estimating spatial patterns in soil organic carbon (Thomas et al., 2020) or air quality (Munir et al., 2019).

Our data-driven methodology is grounded in our process understanding. UHIIs are largely controlled by background climate, e.g. wind speed and cloud cover (Zhao et al., 2014), or city size (Oke, 1973). Faster wind speeds or increased cloud cover are effectively proxies for a well-mixed boundary layer that can efficiently transport heat away from cities (Bassett et al., 2016), and UHIIs are most pronounced at night during calm, anti-cyclonic conditions. Considering the Atlantic, frontal-driven nature of UK climate (characterised by a high through-flow of different weather conditions), variability in UHII is to be expected. Modifying urban morphology, density, construction materials and sky view factors (radiation trapping) will also change UHIIs. This usually results in warming, despite methods existing to mitigate UHIs, such as cool roofs (Georgescu et al., 2014). However, only a small subset of UHI studies contain suitable temporal observations to assess long-term UHI climatology (e.g. London, UK (Wilby, 2003); Manchester, UK (Levermore et al., 2018); New York, U.S. (Gaffin et al., 2008); Reno, U.S. (Hatchett et al., 2016); Rome, Italy (Salvati et al., 2019); Toronto, Canada (Mohsin and Gough, 2010); Turin, Italy (Garzena et al., 2019)).

In London, UK St. James's Park weather station has urban observation records since 1903. Considering the land use immediately surrounding the station has not experienced major changes since pre 1900, it is ideally suited to defining and exploring a long-term UHI climatology. For instance, trend analysis at St James's Park by Wilby (2003) showed a spring and summer nocturnal UHII warming of 0.12 °C decade^{-1} between 1959 and 1998. Conversely, later analysis by Jones and Lister (2009) and Wilby et al. (2011) did not find any trends (1903–2006), finding that St James's Park is warming at the same rate as surrounding rural stations. Wilby et al. (2011) additionally reconstructed a UHII time series at St James's Park back to 1880 using Lamb's (1972) weather classification as predictors, although their method was unable to capture all the variability in UHIIs, explaining only half the variance. Critically, we argue that the methods used in these long-term studies at St James's Park (and the other cities listed above) are unable to distinguish if long-term changes in UHII are urbanisation or climate driven. Surface instrumentation UHII calculation requires both urban and rural references that are reliable and long term. While urbanisation at St James's Park largely occurred pre 1900, this same case cannot be made for the rural reference stations used in their analysis. Reference stations are often compromised in UHI studies, such as by downwind urban heat advection that can extend a cities warming influence far beyond its boundaries (Bassett et al., 2016; see also discussion by Martin-Vide et al. (2015)). The UK, like many other global regions, is also experiencing rapid rural to urban land-use change (Bassett et al., 2020; Chowienczyk et al., 2020) and this may impact the rural references used in these studies (we confirm this in Section 2.2). For the St James's Park station, anthropogenic heat fluxes will have changed over the last century (e.g., the introduction of motorised vehicles), despite the physical built infrastructure remaining constant around. Furthermore, as we report below, the St James's Park weather station contains temporal observational inhomogeneities that will limit interpretations from these earlier analyses.

Here, we take a novel data-driven approach to reconstruct a UHII time series in central London between 1950 and 2019 to overcome limitations of previous studies. We firstly build and test a GAM to learn the relationships between the UHII data in London and independent atmospheric variables like wind speed over a 10-year period. We use the resulting GAM to hindcast UHII a 70-year period where UHII observations are not available, allowing us to explore long-term trends in UHII and apply extreme value theory to the time series. This is made possible by using the ERA5 re-analysis climate data for the independent predictor variables in the model, that is available from 1950 onwards. Through use of ERA5 re-analysis data in substitution of the more traditional (but compromised) rural reference station in our UHII calculation, our analysis is independent of rapid urbanisation effects currently occurring in Great Britain (Bassett et al., 2020). This allows us to make an assessment of changes in UHII in London over time that are driven solely by changes in background climate. The method we present is highly reproducible and can be equally applied to extend UHII time series in other cities globally, where suitable data are available.
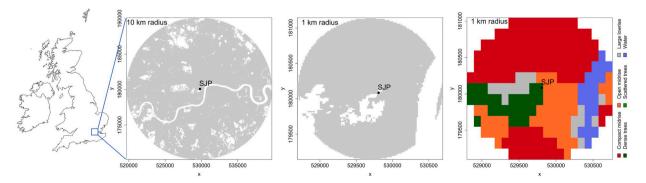

Fig. 1. Location of SJP weather station with surrounding urban land use (grey) in 10 km (left) and 1 km radiuses (middle) using the GHS 2014 built data and 1 km radius for LCZs (right) using mapping from Demuzere et al. (2019).

2. Methods

2.1. Data sources

Air temperature data for London were taken from the UK Met Office weather station in St James' Park, (Met Office, 2019), herein referred to as SJP. The location of the SJP station (51.5048° N, 0.13109° W, 5 m elevation) is shown in Fig. 1. SJP has long records dating back to 1903. For our purposes we require hourly data and find adequate records since 1997, providing a 23-year period to base our analysis on. Despite presenting our final analysis at a monthly time resolution, we built our model from hourly data; the largest UHI intensities are found at night, and a daily value for minimum and maximum temperatures will not capture this.

Global gridded climate observations were taken from the ECMWF ERA5 atmospheric reanalysis at 0.25° (~25 km) resolution, available hourly from 1950 (Hersbach et al., 2018). Climate reanalysis products use data assimilation to combine model forecasts and observations to provide a consistent, although not error free, record of the recent state of the atmosphere. We extracted the following surface variables: 2 m air temperature, total cloud cover, 10 m wind speed and mean sea level pressure. We additionally downloaded 2 m dewpoint temperature and used this to calculate relative humidity.

2.2. UHI intensity calculation

We defined London's UHII as the air temperature difference between SJP and the ERA5 reanalysis data. SJP is located on the right edge of the overlying grid cell, therefore we took the mean of the overlying cell and the adjacent cell to the right for the ERA5 baseline. We interpreted ERA5 as the background "rural" temperature. Note, ERA5 is at a horizontal resolution of ~25 km and only a representation of what the background rural temperatures might be without the presence London. Therefore, the resulting UHII or urban effect on climate presented in this paper should be interpreted as a temperature anomaly and not the absolute UHII for London.

Our observation minus reanalysis approach has been adopted in previous studies exploring the impacts of urbanisation on UHII (e. g. Kalnay and Cai, 2003; Zhou et al., 2004; Goddard and Tett, 2019; Wang et al., 2017). The theory is that reanalysis data is independent of land surface processes like urbanisation. Indeed, ECMWF's model currently represents urban surfaces as either grassland or forest, although an upgrade to include urban processes is anticipated (Hogan et al., 2017). However, we concede that the London ERA5 grid cell may still contain an urban bias from the surface observations used in the data assimilation process. We checked this by plotting the night-time (16:00–08:00) mean temperature across the UK between 1950 and 2020, where we do not see any urban warming impact on ERA5 by comparing London to surroundings (see Supplementary Fig. S1). We would expect to see the grid cells in and around Greater London to be warmer than surroundings (and similarly for other UK cities) if an urban bias is present. This is not the case, thus ERA5 is considered a suitable rural baseline.

Although the SJP station has recorded UHIs up to 7 °C (Wilby, 2003), we also concede that the park location of SJP may lower UHIIs relative to surroundings. Indeed the local climate zone (LCZ; Stewart and Oke, 2012) classification at SJP is scattered trees (data from Demuzere et al., 2019). However, representative observations in the urban environment is a known challenge (Muller et al., 2013) and most urban stations will be compromised to a degree, such as being located on roof tops. The SJP station is located at one end of a park, approximately 100 m to boundary with urban land use (see Fig. 1). At this distance the air will be well mixed with the additional warmth from the surroundings. Furthermore, in the 1 km radius surrounding SJP LCZs are primarily urban, constituting of: compact midrise (50.0%), open midrise (21.6%), scattered trees (11.3%), water (9.0%), large lowrise (7.7%) and dense trees (0.45%); see Fig. 1. A 3D satellite image of SJP's surroundings is provided for further reference in Supplementary Fig. S2. Using data from the 2014 Global Human Settlement (GHS) built layer (Corbane et al., 2018), we additionally calculated an urban fraction (0 rural / 1 urban) of 0.84 from the urban land use in a 1 km radius surrounding SJP, shown in Fig. 1. GHS is a 38 m resolution global urban land use dataset derived from Landsat images covering the periods 1975, 1990, 2000 and 2014.

While the immediate land use surrounding SJP has remained constant since before 1900 (Jones and Lister, 2009), the GHS data further enables us to check for urbanisation around SJP in the last few decades. In a 1 km radius from SJP the urban fractions are 0.82, 0.83, 0.83 and 0.84 for 1975, 1990, 2000 and 2014 respectively, and for a 10 km radius 0.85, 0.86, 0.86, and 0.88. Despite GHS data not yet being available after 2014 (at the time of writing), these urban fraction values suggest very little change in urban land use around SJP (1975–2014) and may be within GHS uncertainty (Pesaresi et al., 2016). As the focus of our study is the variability in UHII caused by climate, using a station with little land-use change limits effects from urbanisation-induced warming. A limitation of the GHS data is that it is unable to show changes to anthropogenic heat emissions over time. However, in Section 2.4 we develop our model over only 10 years of observations which will minimise impacts from urbanisation and anthropogenic heat changes.

Within the analysis period, peripheral areas around London have been rapidly urbanising and subsequently warming (Bassett et al., 2020). This will effectively weaken the calculated UHII signal reported by previous long-term observational studies in London (Jones and Lister, 2009; Wilby, 2003; Wilby et al., 2011) due to urbanisation induced warming at their rural reference stations. Using GHS, we checked for urbanisation at the rural reference stations used in these previous long-term UHI analyses in London. At the Wisley station (51.3108°N, 0.47634°W), we found that the urban fraction has increased between 1975 and 2014 from 0.07 to 0.16 in a 1 km radius, and from 0.16 to 0.27 in a 10 km radius. Similarly at Rothamsted (51.8067°N, 0.36017°W), over the same period, the urban fraction increased from 0.17 to 0.26 in a 1 km radius and from 0.15 to 0.19 in a 10 km radius. Considering the urbanisation around these stations, we would expect a resulting warming. Therefore, these stations may not be suitable for a rural reference, nor for analysis of background climate change without accounting for this bias. The use of ERA5 reanalysis data as a baseline in our UHII calculation avoids these issues.

2.3. Station inhomogeneity

We performed two sets of quality control checks on the data. Firstly, following the UHII calculation we note several instances of spurious data with implausible UHIIs. These data points were removed by not including any UHIIs outside the 0.001 and 0.999 quantiles, in addition to 12 h either side of these points. Secondly, we checked the diurnal mean UHII profile for each year at SJP (Supplementary Fig. S3). We found three distinct diurnal profiles corresponding to the time periods 1997–2002, 2003–2009 and 2010–2019. These periods coincide with instrumentation changes at SJP (see station details at archive.ceda.ac.uk/cgi-bin/midas_stations/station_details.cgi.py?id=697&db=midas_stations). We speculate that from 1997 to 2002 the instrumentation was not housed correctly in a radiation shield (e.g., see the UHII spike at 9 am in Supplementary Fig. S3). From 2003, SJP shows a more typical diurnal UHII profile. A further instrumentation change occurred in 2010, and whilst the pattern is similar to the 2003–2009 period, the UHI range is more consistent between each year. Considering these clear periods, we conducted our analysis with data from 2010 onwards only. We note station inhomogeneity in long-term records will lead to an erroneous UHII trend analysis and any similar study should make appropriate data checks.

2.4. Generalized additive model configuration

We used a generalized additive model (GAM) to uncover the relationships between the UHII in SJP and its predictor variables (e.g. wind speed) over a 10-year period at SJP (2010–2019). Here, we use the R package "mgcv" (Wood, 2020) to fit a GAM to the monthly mean maximum night-time UHII. This was calculated for each month by taking the average of daily maximum UHIIs between 16:00 and 08:00, with these hours chosen as they represent the maximum night length in winter and timing of the maximum UHII (see diurnal profiles in Supplementary Fig. S3). The predictors used in the model are the ERA5 variables: 10 m wind speed, mean sea level pressure, 2 m air temperature and relative humidity. Each were calculated as a monthly mean between 16:00 and 08:00 inclusive. Additionally, a monthly mean of the temperature range (maximum – minimum temperature between 16:00 and 08:00) was calculated and included in the GAM. The structure of the GAM is given below.

$$g(UHII) = \beta_0 + s(\text{wind speed}) + s(\text{pressure}) + s(\text{temperature range}) + s(\text{temperature}) + s(\text{relative humidity}) + \varepsilon$$

where β_0 is the intercept; s is the series of unspecified smoothing functions (we use tensor smoothing as the predictors are on different scales); g is the link function (log selected) that relates the mean of the observations to the predictor variables; and ε is the error term in the model. The GAM was configured using a default Gaussian distribution. We also used REML (random effects of maximum likelihood) estimation for smoothing the parameters, with this option being preferable as it reduces incidences of severe undersmoothing (Wood, 2020).

3. Results

This section details the observed UHII at SJP during a 10-year period before using a GAM to learn the UHII behavior and subsequently hindcast a 70-year time series based on ERA5 predictor variables. The time series is then analysed for variability and trends. Our results should be free from urbanisation, and changes to the time series we present are driven by climate drivers only. In reality the UHIIs change as a function of both climate and land use.
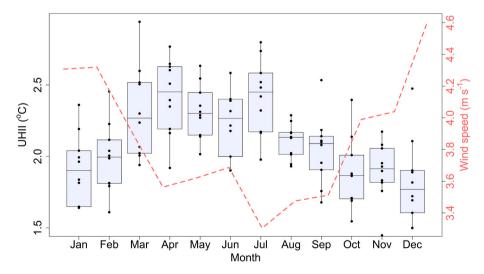

Fig. 2. Distribution of monthly mean maximum UHII for each month. The monthly mean night-time wind speed from ERA5 data is shown as the dashed line. The lines on the boxplots represent 1.5*IQR and dots are the actual UHII values observed in each month.

3.1. Observed urban heat island

We find a mean maximum UHII of 2.11 °C (standard deviation, s.d. 0.80 °C) at SJP over our 10-year analysis period (2010–2019). The UHII maximum is calculated as the largest intensity between 16:00 and 08:00. The all-time daily maximum UHII is 5.07 °C, and daily maximum UHIIs exceeding 3.7 °C occur approximately 18 times per year. As SJP is located in an urban park, albeit near the edge, the UHII in the surrounding urban street canyons may be higher; cities contain a patchwork of internal UHIIs that can be defined by LCZs (Skarbit et al., 2017). For example, observational studies in other UK cities have recorded 8 °C in Birmingham (Bassett et al., 2020) and 10 °C in Manchester (Knight et al., 2010).

Fig. 2 shows the mean maximum UHIIs at a monthly time-resolution together with the monthly mean wind speed. The time series for the observed period can be found in Fig. 4. The largest UHIIs are observed between March and July, with lower UHIIs found in August and September followed by the boreal autumn and winter months. This annual pattern is shown to follow the reverse pattern of monthly mean wind speeds; that is, lower wind speeds occur in the summer months coinciding with larger UHIIs. Fig. 2 also indicates considerable interannual variability. For example, March contains observed monthly mean UHIIs ranging from 1.94 to 2.94 °C within the 10-year data period. The distributions for each month at a daily resolution are provided in Supplementary Fig. S4.

3.2. The GAM

We built a GAM to predict monthly mean maximum UHII, using predictor variables from ERA5 reanalysis (listed in Table 1 along with their individual significance and variable importance). The smoothed predictor variables used in the GAM are shown in Supplementary Fig. S5. We additionally tested running the model including monthly mean cloud cover; however, this was not found to be significant and removed. The fit between the observed and predicted UHIIs is illustrated in Fig. 3, and we achieve an r^2 of 0.82 ($n =$ 120) and a root mean square error of 0.13 °C. Overall we do not find any bias between the GAM model and observations. Prior to running the final GAM configuration, we also tested the model performance by randomly splitting the data into training (80%, $n = 96$) and test (20%, $n = 24$) data sets and subsequently running a new GAM on each. This further highlights the skill of the GAM approach with r^2's between observed and predicted test values ranging between 0.7 and 0.9 (shown in Supplementary Fig. S6).

Over the 10-year period both the observed mean maximum UHII and forecasted are both 2.1 °C. Goddard and Tett (2019), using a comparable observation minus reanalysis method, estimated a similar mean UHII in London of 1.7 °C. A comparison between our reconstructed time series using the GAM and the observed values between 2010 and 2019 is shown in Fig. 4, where the predicted time series closely follows the observed.

3.3. Reconstructed UHII time series

The reconstructed monthly mean maximum UHII time series (referred to as $\overline{UHII'_{max}}$ from here in) from 1950 *to* 2019 that uses the UHII GAM developed in the previous section and with ERA5 reanalysis variables as input is shown in the top row in Fig. 6. The time series data are additionally provided as a supplementary attachment. The length of our hindcasted time series is rare among UHI studies and this allows for a unique insight into UHII trends in the following section.

Across the 70-year time series we find a mean $\overline{UHII'_{max}}$ of 2.09 °C (s.d. 0.25 °C) and considerable inter-annual and seasonal fluctuations, with $\overline{UHII'_{max}}$ ranging between 1.38 and 2.94 °C. To highlight the seasonal variability, the $\overline{UHII'_{max}}$ distributions for each month across the 70-year period are presented in Fig. 5. Within each month, large distributions in $\overline{UHII'_{max}}$ values are found, i.e. each distribution contains 70 months and represents the inter-annual variability. The largest $\overline{UHII'_{max}}$'s are found in April–August (similar to the earlier observed distributions shown in Fig. 2), where mean $\overline{UHII'_{max}}$ are ~2.23 °C. In September–February, $\overline{UHII'_{max}}$ values are ~1.95 °C.

Table 1
Predictor variables used in the daily GAM UHII model. These are night time means (16:00–08:00) with exception of temperature range that is the difference the maximum and minimum temperatures within the same period. The variables are ranked by the F statistic (ratio between the variance explained by the predictors and unexplained variance) which can be used as a proxy for their relative importance in the GAM model. The EDF (effective degrees of freedom) indicates the "wiggliness" of the predictor variables: a value close to 1 would be linear and greater than would be nonlinear (see Supplementary Fig. S5). Significance of the GAM smooth terms: * $p <$ 0.05, ** $p < 0.001$.

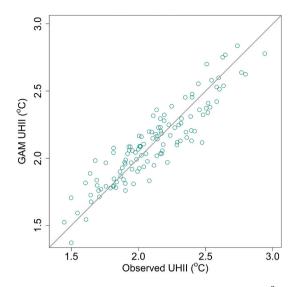|	EDF	F
Wind speed**	1.0	51.1
Temperature**	3.2	26.0
Temperature range**	1.0	25.4
Pressure*	1.1	5.0
Relative humidity*	1.0	4.3

Fig. 3. GAM model performance between observed and predicted monthly mean maximum UHII ($r^2 = 0.82$). The grey line is the 1 to 1 ratio.
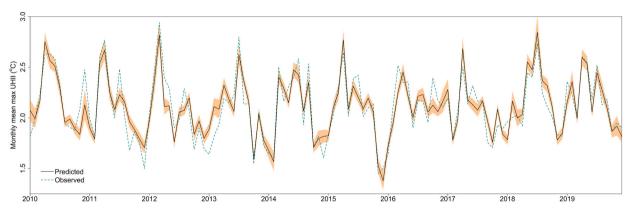

Fig. 4. GAM predicted monthly mean maximum UHII compared with observed between 2010 and 2019. The 95% confidence intervals from the GAM model are provided in orange shading.

3.4. UHII trend

The stationarity of the reconstructed 70-year time series ($\overline{UHII'_{max}}$) was firstly tested using linear regression, where no significant trend was found ($p = 0.24$). Secondly, we decomposed the $\overline{UHII'_{max}}$ time series using the R package "forecast" (Hyndman and Khandakar, 2008). This uses the STL (Seasonal and Trend decomposition using Loess) additive method developed by Cleveland et al. (1990) and splits the time series into seasonal variations, the trend and residuals (i.e. random noise). The results are shown in Fig. 6. We ran a non-parametric Mann-Kendall test (Kendall, 1955) on the time series (1950–2019) where the null hypothesis was accepted ($p = 0.22$), the $\overline{UHII'_{max}}$ time series is stationary.

Although the overall $\overline{UHII'_{max}}$ time series is stationary, we further checked if there is any trend in each season since, for example, opposing summer and winter trends may counteract each other when viewed annually. It is also important to consider seasonal trends separately because adverse UHI impacts are more likely in summer months when background temperatures are already warm. The results show a slight upward $\overline{UHII'_{max}}$ trend in spring and summer months, and decrease in winter months (Fig. 7), although we do not find any significant correlations using linear regression (p: winter 0.06, spring 0.77, summer 0.26, autumn 0.07) nor using the Mann-Kendall test.

3.5. UHII monthly extremes

While the trend in mean UHII has remained stationary, extreme UHIIs are those more likely to adversely impact on society (Santamouris, 2020). We first used a peak over threshold approach. This essentially subsets the time-series to high-magnitude events and enables us to check if the number of these events are increasing or decreasing over time. This approach is similarly used in
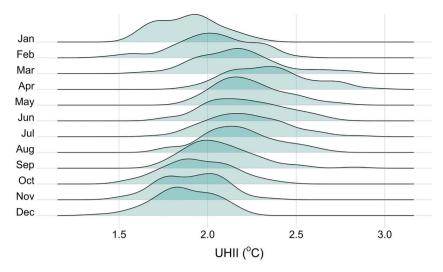
Fig. 5. Monthly $\overline{UHII'_{max}}$ distributions. Each month effectively contains 70 monthly repeats between 1950 and 2019. The vertical axis within each month is the density (a common bandwidth is used for all months).
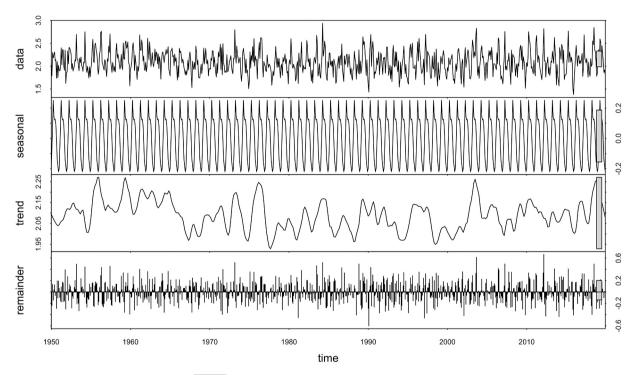

Fig. 6. $\overline{UHII'_{max}}$ time-series decomposition using the R package "forecast".

hydrology (e.g. Janes et al., 2018), yet is less common in UHI analysis due to short observation periods. We show the annual frequency of $\overline{UHII'_{max}}$ exceeding a 75th percentile threshold value of 2.25 °C in Fig. 8. Between 1950 and 2019 the trendline in Fig. 8 suggests a decreasing frequency of extreme UHIIs; however, we do not find this to be significant using linear regression ($p = 0.34$) or the Mann-Kendall test ($p = 0.49$). We note the largest numbers of monthly mean maximum UHIIs exceeding 2.25 °C to occur in the arid (i.e., heatwave / drought) years of 1955, 1959, 1976, 1990, 1995 and 2003; these are highlighted in Fig. 8 and where aridity index values from Marsh et al. (2007) exceed 1.75. Note the 1990 drought extended to 1992. We also test increasing the peak over threshold $\overline{UHII'_{max}}$ value to the 90th percentile of 2.42 °C, shown in Fig. 8, where no significant trends are found.

Although we do not find any significant trend in the 1950–2019 $\overline{UHII'_{max}}$ time series, there is still considerable inter-annual variability (Fig. 6). Considering that UHIs can adversely impact on urban citizens and infrastructure, it is important to understand the likelihood (or return time) of UHIIs exceeding threshold values. To investigate this, we extracted generalized extreme value
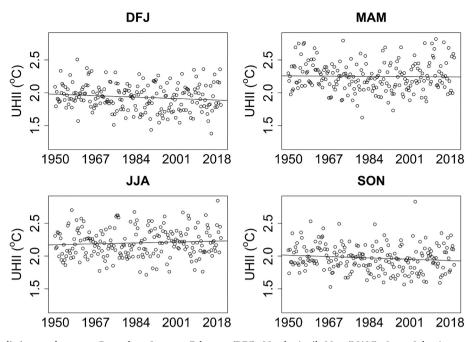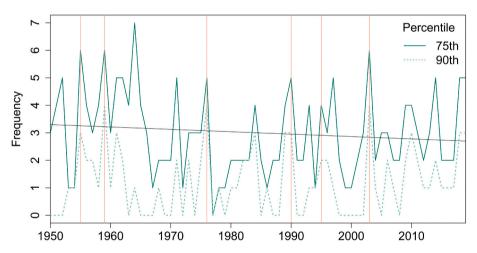
Fig. 7. $\overline{UHII'_{max}}$ split into each season: December, January, February (DFJ); March, April, May (MAM); June, July, August (JJA); September, October, November (SON). While we include the linear regression trend lines, no significant correlations are found in any season.

Fig. 8. Annual frequency of UHIIs exceeding a 75th and 90th percentile peak over threshold $\overline{UHII'_{max}}$ value of 2.25 °C and 2.42 °C respectively. The trendline corresponds to the 75th percentile extremes frequency, however it is not significant. The orange vertical lines correspond to notably arid years.

maximum likelihood estimates on the $\overline{UHII'_{max}}$ time series using the R package "extRemes" (Gilleland and Katz, 2016). This is a further statistical technique used to show the return periods of high-magnitude events, i.e. the tails of distribution. Extreme value analysis is used in the environmental sciences (e.g. Towe et al., 2020; Cheng et al., 2014), but, with exceptions (Steeneveld et al., 2011), it is seldom used for UHI analysis.

The results from the extreme value analysis applied to the $\overline{UHII'_{max}}$ time series are shown in Fig. 9a, using all monthly data points, and Fig. 9b, where they are split seasonally. For all data, we can expect that a $\overline{UHII'_{max}}$ of 2.46 °C will occur once a year on average, while any month exceeding 2.75 °C (99th percentile) would only be expected to occur approximately once in 11 years. Split seasonally, Fig. 9b shows that UHII return periods are smaller in the spring (MAM) and summer (JJA) months. For example, the equivalent annual $\overline{UHII'_{max}}$ return periods for winter months (DJF) are 0.47 °C lower than spring (MAM).
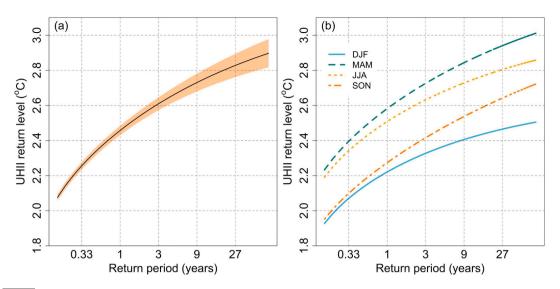
Fig. 9. $\overline{UHII'_{max}}$ return periods. (a) All months included. The orange shading represents the 0.05 confidence intervals. (b) Split into seasons, note confidence intervals are not show.

4. Discussion and conclusions

We have overcome limitations in exploration of long-term UHI changes by using a Generalized Additive Model (GAM) to learn how night-time UHII varies with key predictors at a Central London weather station (St James's Park, SJP) before using the GAM to reconstruct a 70-year time series (1950–2019). The GAM-UHII approach is a significant improvement over earlier attempts to reproduce a UHII time series at SJP. Previously, it was only possible to explain half the variance (Wilby et al., 2011) where, at monthly resolution, our GAM achieved an r^2 of 0.82 ($n = 120$). We acknowledge that there are some limitations to our reconstructed time series. Firstly, our estimates may underestimate the absolute UHII intensity due to the park siting of SJP; an urban fraction of 0.84 is found within a 1 km radius. Therefore, it may be warmer within nearby urban street canyons, hence our stated UHIIs should not be treated as absolute. Secondly, our results are for a single location only and may not be representative of changes in UHII climate drivers in other cities. Finally, while our GAM-UHII method is able to capture the majority of variability in the observed data ($r^2 = 0.82$), our time series analysis is ultimately a reconstruction. Despite long observational records at SJP, hourly back to 1997 and daily to 1903, we found a discontinuity in the hourly observations, these occurring at instrumentation changes. As such our GAM was developed over 10 years of consistent data (2010–2019). A benefit of this shorter period is that it acts to limit longer-term warming from urbanisation or anthropogenic heat changes around the station. Moreover, our checks did not find any notable urbanisation trends immediately surrounding the SJP station in the model development period; our checks showed urban fraction change between 2000 and 2014 was 0.83 to 0.84. Furthermore, the GAM does not use time as a predictor, hence it would not include urbanisation changes at SJP, if any, during this period. Our methodology means the trend in the monthly mean maximum UHII ($\overline{UHII'_{max}}$) reconstructed time series is based on climate drivers only (like wind speed).

We estimate a mean $\overline{UHII'_{max}}$ of 2.09 °C over the reconstructed analysis period. This value is similar to previous estimates for London, albeit using different methods (1.9 °C (Wilby, 2003); 1.6 °C (Jones and Lister, 2009); 1.7 °C (Goddard and Tett, 2019)). However, while past attempts have been made to explore long-term UHII trends and variability (e.g. Wilby et al., 2011), they were unable to differentiate between the different land use and/or climate change drivers of UHII change. We found that the traditional rural references used in previous long-term UHI studies in London are susceptible to urbanisation and therefore need to be evaluated carefully. Throughout our reconstructed time series, considerable variability in UHII was found, both between and within seasons, with $\overline{UHII'_{max}}$ ranging between 1.38 and 2.94 °C (1950–2019). Most UHI studies are too short in length (usually less than a year) to capture these UHII fluctuations (see Figs. 4 and 5); that is, two months are rarely alike. As such, short UHII studies will not adequately represent long-term means and likely miss high-magnitude events. As a caveat, the UK climate is influenced by large, Atlantic driven fluctuations in weather patterns that will drive UHII variability. Other global regions, e.g. more arid areas, may experience less variability in the UHII climate drivers and hence UHII, and therefore shorter study periods may be appropriate.

Over the 70-year $\overline{UHII'_{max}}$ reconstructed time series we did not detect any significant trends in London's UHII, even if the seasons were treated separately; this was tested using both linear regression and the non-parametric Mann-Kendall test. This apparent stationarity of London's UHII is in agreement with previous long-term studies (Jones and Lister, 2009; Wilby, 2003; Wilby et al., 2011). Yet, while those studies argued that the land use at the SJP weather station has not changed since pre 1900, the same is not true for their rural reference stations: London's peripheries are rapidly urbanising. Simultaneously with our reconstructed time series, the ERA5 background 2 m air temperature in London warmed over 1950–2019 at 0.25 °C decade^{-1} (see Supplementary Fig. S7), which is comparable to NOAA estimates (NOAA, 2021). Therefore, our results indicate that the mean UHII in London has not changed despite

moving to a warmer climate. UHII stationarity in other UK cities due to a changing climate has also been reported using regional climate modelling (McCarthy et al., 2012) and little or no change other cities worldwide (Kusaka et al., 2012; Lauwaet et al., 2016). However, future projections contain uncertainty in UHII drivers, summer night-time UHIIs in London have equally been modelled to increase by 2080 (Eunice Lo et al., 2020).

While the overall UHII trend is stationary in London (1950–2019), we used peaks over threshold analysis to check for any change in frequency of high-magnitude events. Over the entire period, despite the trend in extremes over time appearing to increase we did not find this to be significant. We note that years with the highest frequency of high magnitude events occurred in heatwave / drought years, e.g. 2003. This year contained an exceptional heatwave that encompassed most of Europe and resulted in thousands of excess deaths (Robine et al., 2008). Heatwave conditions are characterised by calm conditions that lead to increased UHIIs. Future climate projections indicate there will be an increasing number of similar heatwaves in the UK by 2100 (Christidis et al., 2020). Through applying extreme value analysis to the time series, we estimate the current return period for a $\overline{UHII'_{max}}$ exceeding 2.75 °C (99th percentile) is approximately 11 years. Return periods for high-magnitude events are found to be shorter for spring and summer months; more intense UHIs occurring in periods when background temperatures are already warm mean thresholds for heat risks to vulnerable citizens are more likely to be reached.

Overall, we have developed and shown the effectiveness of applying emerging data-science techniques, in this case a GAM, to complex urban climate data. Through reconstructing a 70-year UHII time series, this has allowed a unique insight into the long-term changes in London's UHII that are solely due to UHII climate drivers. Despite moving to a warmer background climate between 1950 and 2019, we show that the mean UHII has not changed. The simplicity of our approach means it can easily be adapted to other locations, providing that there is enough observational data available to create a GAM or equivalent data science model. Based on our findings we additionally emphasise two important messages to the urban climate community concerning UHI methodologies: (i) UHIIs may have large monthly and annual fluctuations, and short studies will not adequately capture these, and (ii) to fully understand long-term changes in UHII, the drivers of UHII, urbanisation or climate should be treated independently.

Data availability

Data for St James's Park weather station is accessible through the Met Office MIDAS Open: UK Land Surface Stations Data (1853-current) http://catalogue.ceda.ac.uk/uuid/dbd451271eb04662beade68da43546e1

ECMWF ERA5 atmospheric reanalysis data is available from doi:10.24381/cds.bd0915c6

The monthly mean reconstructed UHII time series may be found as a supplementary attachment. All code to reproduce our finds may be obtained from the authors at reasonable request.

Declaration of Competing Interest

The authors declare that they have no known competing financial interests or personal relationships that could have appeared to influence the work reported in this paper.

Acknowledgements

Appendix A. Supplementary data

Supplementary data to this article can be found online at https://doi.org/10.1016/j.uclim.2021.100990.

References

Bassett, R., Cai, X., Chapman, L., Heaviside, C., Thornes, J.E., Muller, C.L., Young, D.T., Warren, E.L., 2016. Observations of urban heat island advection from a high-density monitoring network. Q. J. R. Meteorol. Soc. 142, 2434–2441. https://doi.org/10.1002/qj.2836.

Bassett, R., Young, P.J., Blair, G.S., Cai, X.-M., Chapman, L., 2020. Urbanisation's contribution to climate warming in Great Britain. Environ. Res. Lett. 15, 114014. https://doi.org/10.1088/1748-9326/abbb51.

Cheng, L., AghaKouchak, A., Gilleland, E., Katz, R.W., 2014. Non-stationary extreme value analysis in a changing climate. Clim. Chang. 127, 353–369. https://doi.org/10.1007/s10584-014-1254-5.

Chowienczyk, K., McCarthy, M., Hollis, D., Dyson, E., Lee, M., Coley, D., 2020. Estimating and mapping urban heat islands of the UK by interpolation from the UK Met Office observing network. Build. Serv. Eng. Res. Technol. 41, 521–543. https://doi.org/10.1177/0143624419897254.

Christidis, N., McCarthy, M., Stott, P.A., 2020. The increasing likelihood of temperatures above 30 to 40 °C in the United Kingdom. Nat. Commun. 11, 3093. https://doi.org/10.1038/s41467-020-16834-0.

Cleveland, R.B., Cleveland, W.S., McRae, J.E., Terpenning, I., 1990. STL: a seasonal-trend decomposition. J. Off. Stat. 6 (1), 3–73.

Corbane, C., Florczyk, A., Pesaresi, M., Politis, P., Syrris, V., 2018. GHS Built-up Grid, Derived from Landsat, Multitemporal (1975–1990–2000-2014), R2018A. European Commission, Joint Research Centre (JRC). https://doi.org/10.2905/jrc-ghsl-10007 PID. http://data.europa.eu/89h/jrc-ghsl-10007.

Demuzere, M., Bechtel, B., Middel, A., Mills, G., 2019. Mapping Europe into local climate zones. PLoS One 14, e0214474. https://doi.org/10.1371/journal.pone.0214474.

Eunice Lo, Y.T., Mitchell, D.M., Bohnenstengel, S.I., Collins, M., Hawkins, E., Hegerl, G.C., Joshi, M., Stott, P.A., 2020. U.K. climate projections: summer daytime and nighttime urban heat island changes in England's major cities. J. Clim. 33, 9015–9030. https://doi.org/10.1175/JCLI-D-19-0961.1.

Gaffin, S.R., Rosenzweig, C., Khanbilvardi, R., Parshall, L., Mahani, S., Glickman, H., Goldberg, R., Blake, R., Slosberg, R.B., Hillel, D., 2008. Variations in New York city's urban heat island strength over time and space. Theor. Appl. Climatol. 94, 1–11. https://doi.org/10.1007/s00704-007-0368-3.

Garzena, D., Acquaotta, F., Fratianni, S., 2019. Analysis of the long-time climate data series for Turin and assessment of the city's urban heat island. Weather 74, 353–359. https://doi.org/10.1002/wea.3292.

Georgescu, M., Morefield, P.E., Bierwagen, B.G., Weaver, C.P., 2014. Urban adaptation can roll back warming of emerging megapolitan regions. Proc. Natl. Acad. Sci. U. S. A. 111, 2909–2914. https://doi.org/10.1073/pnas.1322280111.

Gilleland, E., Katz, R.W., 2016. extRemes 2.0: an extreme value analysis package in R. J. Stat. Softw. 72 (8), 1–39. https://doi.org/10.18637/jss.v072.i08.

Goddard, I.L.M., Tett, S.F.B., 2019. How much has urbanisation affected United Kingdom temperatures? Atmos. Sci. Lett. 20, e896 https://doi.org/10.1002/asl.896.

Hatchett, B.J., Koračin, D., Mejía, J.F., Boyle, D.P., 2016. Assimilating urban heat island effects into climate projections. J. Arid Environ. 128, 59–64. https://doi.org/10.1016/j.jaridenv.2016.01.007.

Hersbach, H., Bell, B., Berrisford, P., Biavati, G., Horányi, A., Muñoz Sabater, J., Nicolas, J., Peubey, C., Radu, R., Rozum, I., Schepers, D., Simmons, A., Soci, C., Dee, D., Thépaut, J.-N., 2018. ERA5 hourly data on single levels from 1979 to present. In: Copernicus Climate Change Service (C3S) Climate Data Store (CDS). https://doi.org/10.24381/cds.adbb2d47 (Accessed on 01-10-2020).

Hogan, R.J., Ahlgrimm, M., Balsamo, G., Beljaars, A., Berrisford, P., Bozzo, A., Di Giuseppe, F., Forbes, R.M., Haiden, T., Lang, S., Mayer, M., 2017. Radiation in Numerical Weather Prediction. European Centre for Medium-Range Weather Forecasts.

Hyndman, R.J., Khandakar, Y., 2008. Automatic time series forecasting: the forecast package for R. J. Stat. Softw. 26 (3), 1–22. https://doi.org/10.18637/jss.v027.i03.

Janes, V., Holman, I., Birkinshaw, S., O'Donnell, G., Kilsby, C., 2018. Improving bank erosion modelling at catchment scale by incorporating temporal and spatial variability. Earth Surf. Process. Landf. 43, 124–133. https://doi.org/10.1002/esp.4149.

Jones, P.D., Lister, D.H., 2009. The urban heat island in Central London and urban-related warming trends in Central London since 1900. Weather 64, 323–327. https://doi.org/10.1002/wea.432.

Kalnay, E., Cai, M., 2003. Impact of urbanization and land-use change on climate. Nature 423, 528–531. https://doi.org/10.1038/nature01675.

Kendall, M.G., 1955. Rank Correlation Methods, 2nd ed. Hafner Publishing Co.

Knight, S., Smith, C., Roberts, M., 2010. Mapping Manchester's urban heat island. Weather 65, 188–193. https://doi.org/10.1002/wea.542.

Kusaka, H., Masayuki, H., Takane, Y., 2012. Urban climate projection by the WRF model at 3-km horizontal grid increment: dynamical downscaling and predicting heat stress in the 2070's August for Tokyo, Osaka, and Nagoya metropolises. J. Meteorol. Soc. Japan. Ser. II 90B, 47–63. https://doi.org/10.2151/jmsj.2012-B04.

Lamb, H.H., 1972. British Isles weather types and a register of the daily sequence of circulation patterns 1861–1971. In: Meteorological Office Memoir 116. HMSO, London.

Lauwaet, D., De Ridder, K., Saeed, S., Brisson, E., Chatterjee, F., van Lipzig, N.P.M., Maiheu, B., Hooyberghs, H., 2016. Assessing the current and future urban heat island of Brussels. Urban Clim. 15, 1–15. https://doi.org/10.1016/j.uclim.2015.11.008.

Levermore, G., Parkinson, J., Lee, K., Laycock, P., Lindley, S., 2018. The increasing trend of the urban heat island intensity. Urban Clim. 24, 360–368. https://doi.org/10.1016/j.uclim.2017.02.004.

Marsh, T., Cole, G., Wilby, R., 2007. Major droughts in England and Wales, 1800–2006. Weather 62, 87–93. https://doi.org/10.1002/wea.67.

Martin-Vide, J., Sarricolea, P., Moreno-GarcÃ-a, M.C., 2015. On the definition of urban heat island intensity: the "rural" reference. Front. Earth Sci. 3, 2–4. https://doi.org/10.3389/feart.2015.00024.

Masson, V., Lemonsu, A., Hidalgo, J., Voogt, J., 2020. Urban climates and climate change. Annu. Rev. Environ. Resour. 45, 411–444. https://doi.org/10.1146/annurev-environ-012320-083623.

Mccarthy, M.P., Harpham, C., Goodess, C.M., Jones, P.D., 2012. Simulating climate change in UK cities using a regional climate model, HadRM3. Int. J. Climatol. 32, 1875–1888. https://doi.org/10.1002/joc.2402.

Met Office., 2019. Met Office MIDAS Open: UK Land Surface Stations Data (1853-current). Centre for Environmental Data Analysis, 29 March 2021. http://catalogue.ceda.ac.uk/uuid/dbd451271eb04662beade68da43546e1.

Mohsin, T., Gough, W.A., 2010. Trend analysis of long-term temperature time series in the Greater Toronto area (GTA). Theor. Appl. Climatol. 101, 311–327. https://doi.org/10.1007/s00704-009-0214-x.

Muller, C.L., Chapman, L., Grimmond, C.S.B., Young, D.T., Cai, X.-M., 2013. Toward a standardized metadata protocol for urban meteorological networks. Bull. Am. Meteorol. Soc. 94, 1161–1185. https://doi.org/10.1175/BAMS-D-12-00096.1.

Munir, S., Mayfield, M., Coca, D., Jubb, S.A., Osammor, O., 2019. Analysing the performance of low-cost air quality sensors, their drivers, relative benefits and calibration in cities—a case study in Sheffield. Environ. Monit. Assess. 191, 94. https://doi.org/10.1007/s10661-019-7231-8.

NOAA, 2021. National Centers for Environmental information, Climate at a Glance: Global Time Series. published March 2021, retrieved on March 29, 2021 from. https://www.ncdc.noaa.gov/cag/.

Oke, T.R., 1973. City size and the urban heat island. Atmos. Environ. 7, 769–779. https://doi.org/10.1016/0004-6981(73)90140-6.

Pesaresi, M., Ehrlich, D., Ferri, S., Florczyk, A.J., Freire, S., Halkia, M., Julea, A., Kemper, T., Soille, P., Syrris, V., 2016. Operating Procedure for the Production of the Global Human Settlement Layer from Landsat Data of the Epochs 1975, 1990, 2000, and 2014. https://doi.org/10.2788/253582.

Robine, J.M., Cheung, S.L.K., Le Roy, S., Van Oyen, H., Griffiths, C., Michel, J.P., Herrmann, F.R., 2008. Death toll exceeded 70,000 in Europe during the summer of 2003. Comp. Rendus Biol. 331, 171–178. https://doi.org/10.1016/j.crvi.2007.12.001.

Salvati, L., Zambon, I., Pignatti, G., Colantoni, A., Cividino, S., Perini, L., Pontuale, G., Cecchini, M., 2019. A time-series analysis of climate variability in urban and agricultural sites (Rome, Italy). Agriculture 9, 103. https://doi.org/10.3390/agriculture9050103.

Santamouris, M., 2020. Recent progress on urban overheating and heat island research. Integrated assessment of the energy, environmental, vulnerability and health impact. Synergies with the global climate change. Energy Build. 207 https://doi.org/10.1016/j.enbuild.2019.109482.

Skarbit, N., Stewart, I.D., Unger, J., Gál, T., 2017. Employing an urban meteorological network to monitor air temperature conditions in the 'local climate zones' of Szeged, Hungary. Int. J. Climatol. 37, 582–596. https://doi.org/10.1002/joc.5023.

Steeneveld, G.J., Koopmans, S., Heusinkveld, B.G., van Hove, L.W.A., Holtslag, A.A.M., 2011. Quantifying urban heat island effects and human comfort for cities of variable size and urban morphology in the Netherlands. J. Geophys. Res. 116, D20129 https://doi.org/10.1029/2011JD015988.

Stewart, I.D., Oke, T.R., 2012. Local climate zones for urban temperature studies. Bull. Am. Meteorol. Soc. 93, 1879–1900. https://doi.org/10.1175/BAMS-D-11-00019.1.

Thomas, A., Cosby, B.J., Henrys, P., Emmett, B., 2020. Patterns and trends of topsoil carbon in the UK: complex interactions of land use change, climate and pollution. Sci. Total Environ. 729, 138330. https://doi.org/10.1016/j.scitotenv.2020.138330.

Towe, R., Tawn, J., Eastoe, E., Lamb, R., 2020. Modelling the clustering of extreme events for short-term risk assessment. J. Agric. Biol. Environ. Stat. 25, 32–53. https://doi.org/10.1007/s13253-019-00376-0.

Wang, J., Tett, S.F.B., Yan, Z., 2017. Correcting urban bias in large-scale temperature records in China, 1980-2009. Geophys. Res. Lett. 44, 401–408. https://doi.org/10.1002/2016GL071524.

Wilby, R.L., 2003. Past and projected trends in London's urban heat island. Weather 58, 251–260. https://doi.org/10.1256/wea.183.02.

Wilby, R.L., Jones, P.D., Lister, D.H., 2011. Decadal variations in the nocturnal heat island of London. Weather 66, 59–64. https://doi.org/10.1002/wea.679.

Wood, S.N., 2020. Package "mgcv". Retrieved from. https://cran.r-project.org/web/packages/mgcv/mgcv.pdf.

Zhao, L., Lee, X., Smith, R.B., Oleson, K., 2014. Strong contributions of local background climate to urban heat islands. Nature 511, 216–219. https://doi.org/10.1038/nature13462.

Zhou, L., Dickinson, R.E., Tian, Y., Fang, J., Li, Q., Kaufmann, R.K., Tucker, C.J., Myneni, R.B., 2004. Evidence for a significant urbanization effect on climate in China. Proc. Natl. Acad. Sci. 101, 9540–9544. https://doi.org/10.1073/pnas.0400357101.